J Electroceram (2007) 18:329–337
DOI 10.1007/s10832-007-9129-z

Solid state rapid quenching method to synthesize micron size $Li_4Ti_5O_{12}$

M. Ganesan · M. V. T. Dhananjeyan · K. B. Sarangapani · N. G. Renganathan

Received: 26 July 2006 / Accepted: 9 April 2007 / Published online: 2 June 2007

Abstract $Li_4Ti_5O_{12}$ spinel has been synthesized by a new solid-state rapid quenching method adopting solid-state synthesis followed by quenching leading to stoichiometric phase pure micron size material. By simple freezing of the solid-state reaction occurring at 800 °C using ice cold medium, micron sized particulates are achieved. The powder has been characterized by X-ray diffraction, SEM, etc. By this synthesis uniform morphology has been attained and particle size of fine particulates of $Li_4Ti_5O_{12}$ of an average size of 1–2 μm has been achieved. High rate characteristic and excellent cyclability are the highlights of newly synthesized material. Diffusion coefficient of Lithium has been evaluated and it is found to be 1.4×10^{-15} cm^2 s^{-1}. A maximum reversible lithium insertion capacity of 154 $mAhg^{-1}$ at 2 C rate has been achieved. Results are discussed in this paper.

Keywords $Li_4Ti_5O_{12}$ · Quench method · Cyclic voltammetry · a.c. impedance · Charge–discharge · Dielectric

1 Introduction

In high energy density batteries, lithium metal is a very attractive material because of its low equivalent weight and high constant voltage. At the same time, the high reactivity of lithium restricts its use as anode in real batteries, and rechargeable lithium batteries failed to be introduced into the market due to safety concerns. The introduction of carbonaceous materials solved in part the safety problems related to lithium metal and allowed the large-scale commercialization of the so-called lithium ion battery technology. Lithium intercalation compounds are used in rocking chair rechargeable batteries for the positive and negative electrodes. The low cost materials with high performance are essential for these batteries. Concerning new anodic materials that are able to intercalate lithium at higher voltages, cobalt nitrides [1], manganese nitrides [2] and transition metal oxides characterized by a low intercalation potential such as WO_2 and MoO_2 [3], Nb_2O_3 [4], $Li_4Mn_5O_{12}$, $Li_{12}Mn_4O_9$ [5], TiO_2 [6] and $CuCoS_3O_8$ [7] have received great attention, together with several lithium titanates both with ramsdellite structure [8, 9] and spinel structure [10]. Cyclability of electrodes used in Lithium Secondary batteries greatly depends on the structural stability of the host materials during the Charge–Discharge process.

Ohzuku et al. have identified $Li_4Ti_5O_{12}$ as a zero strain material with excellent cyclability [10]. $Li_4Ti_5O_{12}$ spinel can be considered as a good negative electrode for solid-state lithium batteries due to its very flat charge and discharge curves and high cyclability [10–23]. This material has a theoretical specific capacity of 175 $mAhg^{-1}$ and exhibited a practical specific capacity as high as 160 $mAhg^{-1}$ after 100 deep discharge cycles. The mid-discharge potential for Li insertion is about 1.5 V vs. Li, which is above the potential range where most electrolytes or solvents are reduced. This material was successfully used as anode coupled with promising cathode material such as $LiMn_2O_4$ or $LiCoO_2$ to provide a cell with an operating voltage of about 2.5 V [18, 24].

M. Ganesan · M. V. T. Dhananjeyan · K. B. Sarangapani · N. G. Renganathan
Central Electro Chemical Research Institute, Karaikudi, India

M. Ganesan (✉)
Electrochemical Energy systems Division, CECRI, Karaikudi 630006, India
e-mail: mgshan2002@yahoo.co.in

The spinel $Li_4Ti_5O_{12}$ was prepared by solid-state reaction of stoichiometric amounts of TiO_2 and Li_2CO_3 or TiO_2 and LiOH, heating at 800–1,000 °C for 12–24 h [25–33]. Zaghib et al. prepared nanocrystalline $Li_4Ti_5O_{12}$ of particle size 600 nm by simple high energy grinding of the microcrystalline spinel using a ball mill. However, the electrochemical performance was not significantly different among their materials [31]. Amatucci et al. have recently reported on nanocrystalline $Li_4Ti_5O_{12}$ exhibiting a very promising charging rate and stability in an asymmetric hybrid cell with a super capacitor cathode. $Li_4Ti_5O_{12}$ resulted from a high temperature solid-state reaction of TiO_2 and Li_2CO_3 was used as the anode in the above device, but neither the particle size nor preparative details were specified in their works [34, 35].

Recently several attempts were made to grow nanocrystalline $Li_4Ti_5O_{12}$ (spinel) by the sol–gel method from lithium acetate and titanium (IV) iso-propoxide or butoxide [36, 37]. The sol–gel product from the butoxide route exhibited a grain size of 100 nm, but the product contains some rutile impurities. The high temperature solid-state reaction is usually selected for the synthesis of $Li_4Ti_5O_{12}$ [25, 26].

In this paper, synthesis of $Li_4Ti_5O_{12}$ has been made by solid-state reactions of ball milled Li_2CO_3 and TiO_2 and quenching the molten mass suddenly with a view to reduce the particle size. For the first time this method of preparation is adopted to synthesize $Li_4Ti_5O_{12}$. Characterization of this material by thermal analysis, particle size distribution, XRD and SEM has been made. Electrochemical charge–discharge, Cyclic Voltammetry and Impedance have been done and results are presented in this communication.

2 Experimental

Synthesis of $Li_4Ti_5O_{12}$ was carried out with starting materials of high purity of TiO_2 (E. Merck) and Li_2CO_3 (E. Merck). TiO_2 and Li_2CO_3 was initially ball milled for 15 h prior to mixing stoichiometrically. Stoichiometry mixture corresponding to $Li_4Ti_5O_{12}$ was ball milled with acetone at room temperature for 15 h. The powders were dried at 90 °C for 8 h and fired at 900 °C for 24 h. The molten mass was suddenly quenched at ice-cold medium and reground. The structure and morphology properties of the precursors and oxide powders were characterized by several techniques. X-ray diffraction (XRD) data were collected using a JEOL-JDX 8030 X-ray diffractometer, λ=1.5406 A° using nickel filtered Cu kα. Particle size distribution was carried out using Horiba LA-910 Laser scattering particle size analyzer. Thermogravimetric and differential thermal analysis (TG/DTA) were performed using STA 1500 Thermal analyzer at a heating rate of 20 °C min^{-1}. Surface morphology of the compound was characterized by Hitachi S 3000 H Scanning electron Microscope. The BET surface area of the prepared material was determined from Nitrogen adsorption isotherm at 77 K (Quanta Chrome Nova 1000, US).

Electrochemical studies were carried out using 2016 coin cell assembled inside a glove box. Autolab PGSTAT 30 controlled by GPES—4.9 software was used. The electrolyte solution used was EC, DMC (1:1) mixture with $LiPF_6$. The experiments were carried out in two electrode cell configuration where the reference and auxiliary electrodes were Li metal. In these type of experiments Li metal acts as quasi reference and auxiliary electrodes and all potentials are referred to this potential which is taken as Li/Li^+ reference electrode. The anode was prepared by coating lithium titanium oxide (85%) mixed with 10% of acetylene black and 5% PVDF as a binder over aluminum foil. Impedance spectroscopy was carried out in the frequency range 1 mHz–100 kHz by using Autolab PGSTAT 30. Dielectric constant and dissipation factor were evaluated using impedance parameters. A computer controlled Bitrode USA life cycle tester was used for cycle tests at constant current.

3 Results and discussion

3.1 TGA/DTA

Figure 1 shows the TG/DTA curve (from 20 to 900 °C) of $Li_4Ti_5O_{12}$ precursor and this enables to follow its kinetics of formation. The total mass loss was 11%. Two distinct steps of weight loss were observed on the TG curve of the precursor powder. The first step is obviously due to the vaporization of water and loss of carbonates. An endothermic peak around 500 °C on the DTA curve has appeared. The energy of activation was estimated using McGarty and Green Kinetics and it was found to be 153.56 Kcal/mole. The second step in TG curve in the temperature range 640–800 °C indicates the phase change reaction of TiO_2 and the formation of crystalline phase. A small weak endothermic peak appeared around 650 °C in DTA curve can be ascribed to the anatase—rutile transformation before formation of the spinel phase $Li_4Ti_5O_{12}$. and the heat of formation is indicated below.

$$TiO_2(\text{Anatase}) \rightarrow TiO_2(\text{Rutile}), \Delta H = 0.39\,\text{cal/mole}.$$

As expected, in this temperature range there is no appreciable amount of weight loss is noted. Since in this temperature range only conversion of anatase to rutile happens leading to the formation of $Li_4Ti_5O_{12}$. The minimum formation temperature of $Li_4Ti_5O_{12}$ is around 600 °C and the phase pure $Li_4Ti_5O_{12}$ can be obtained by heating the sample up to 800 °C.

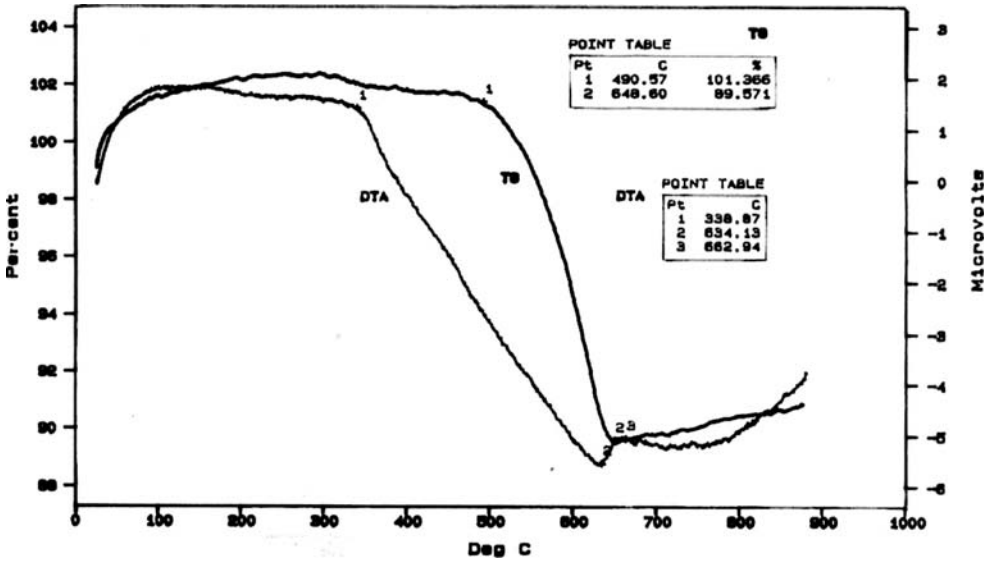

Fig. 1 TG/DTA curve of $Li_4Ti_5O_{12}$ precursor powder

3.2 XRD studies

The formation of phase pure crystalline $Li_4Ti_5O_{12}$ can be seen from the XRD pattern fired at 800 °C. The XRD pattern, shown in Fig. 2, correlates well with that reported for $Li_4Ti_5O_{12}$ having spinel framework structure. The XRD pattern in Fig. 2 reveals all the characteristics diffraction peaks such as (111), (311), (400), (511) and (440) diffraction phases of spinel $Li_4Ti_5O_{12}$ crystal. The absence of principal peak, characteristics of TiO_2 localized at 2θ Bragg angle at 25.28° in the product, indicates the complete conversion of TiO_2 in the solid-state reaction. The sharpness of the main peak that appeared at 2θ=18.36° indicates high crystallinity of the synthesized powder. As per DTA, the $Li_4Ti_5O_{12}$ crystal phase began to form at 600 °C and it is completed at 800 °C. The lattice parameter of the synthesized compound was 8.368 A°. The XRD pattern agree well with the reported $Li_4Ti_5O_{12}$ and it has a defective spinel framework structure with a=8.368 A°. It is in agreement with Ohzuku et al. [10] (8.367 A°) and Colbow et al. [26] (8.365 A°). The value is also similar to the lattice constant of 0.8359 nm calculated from the JCP2 CAT pattern (PDF.no-26-1198).

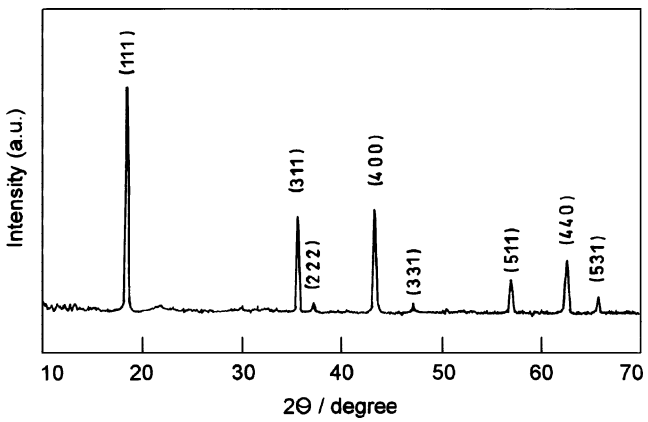

Fig. 2 XRD pattern of $Li_4Ti_5O_{12}$

3.3 SEM and particle size distribution

SEM images of $Li_4Ti_5O_{12}$ crystals are shown in Fig. 3. It is apparent that $Li_4Ti_5O_{12}$ exhibits regular uniform particles with good dispersivity. From the figure it appears that $Li_4Ti_5O_{12}$ displays evenly distributed fine particles with small agglomerates. The particle sizes by SEM were reasonably comparable to the values calculated from the Eq. 1.

$$d_p = 6/\rho S_{\mathrm{BET}} \tag{1}$$

where d—particle size, ρ—density and S_{BET}—Surface area of the particle estimated from BET area.

The average particle size was estimated by assuming non-porous spherical grains of a density ρ=3.5 g/cm^3 .(The

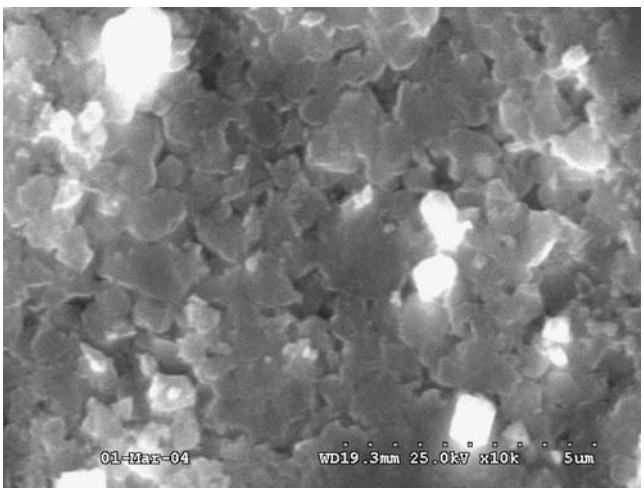

Fig. 3 SEM picture of $Li_4Ti_5O_{12}$

density of the material is determined independently by the standard methods adopted in physics (S.G. method). Hence the average particle size of the particles calculated from the above Eq. 1 is about 0.28 μm.

The dimensions of $Li_4Ti_5O_{12}$ crystallites were obtained from the full width half maxima of peaks observed in Fig. 2 using Scherrer formula

$$D = \beta\lambda/B\mathrm{Cos}\theta, \quad (2)$$

Where D_{hkl} is the linear dimension of the coherent diffraction along a direction normal to the diffraction plane (hkl), λ—X-ray wavelength (1.5418 A°), β—the crystal shape constant (0.89), θ—the reflection angle of the peak, and B is the corrected full width at half maximum (FWHM) of the peak in radians. Calculated from the width of the XRD reflection peaks, the dimension of $Li_4Ti_5O_{12}$ crystallites are 240 nm (111), 337 nm (311), 620 nm (400) and 200 nm (440), respectively.

From the Fig. 4, the average particle size of $Li_4Ti_5O_{12}$ determined by the laser diffraction-scattering method is 1.72 μm, exhibiting the coefficient of variation (CV) on a volume basis. The particle size of the powder was uniformly distributed between 1.0 and 2.0 μm. The specific surface area was determined by the BET method and it is found to be 5.2 m^2/g.

4 Electro chemical studies

4.1 Cyclic voltammetry studies

The electrochemical properties of $Li_4Ti_5O_{12}$ sample was evaluated with cyclic voltammetry (CV) with an electrode area of 1 cm^2 having an active electrode material of 20 mg in a mixed solvent of ethylene carbonate and dimethyl carbonate (1:1) containing 1.0 $moldm^{-3}$ of $LiPF_6$. Figure 5(a) and (b) show a cyclic voltammogram of $Li_4Ti_5O_{12}$ sample. The voltage was initially scanned from

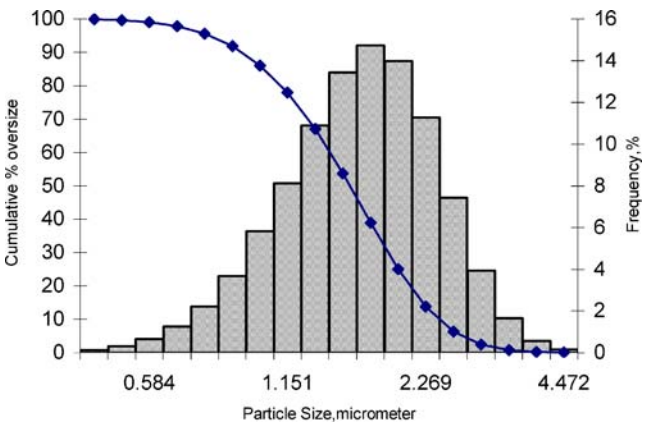

Fig. 4 Particle size distribution $Li_4Ti_5O_{12}$

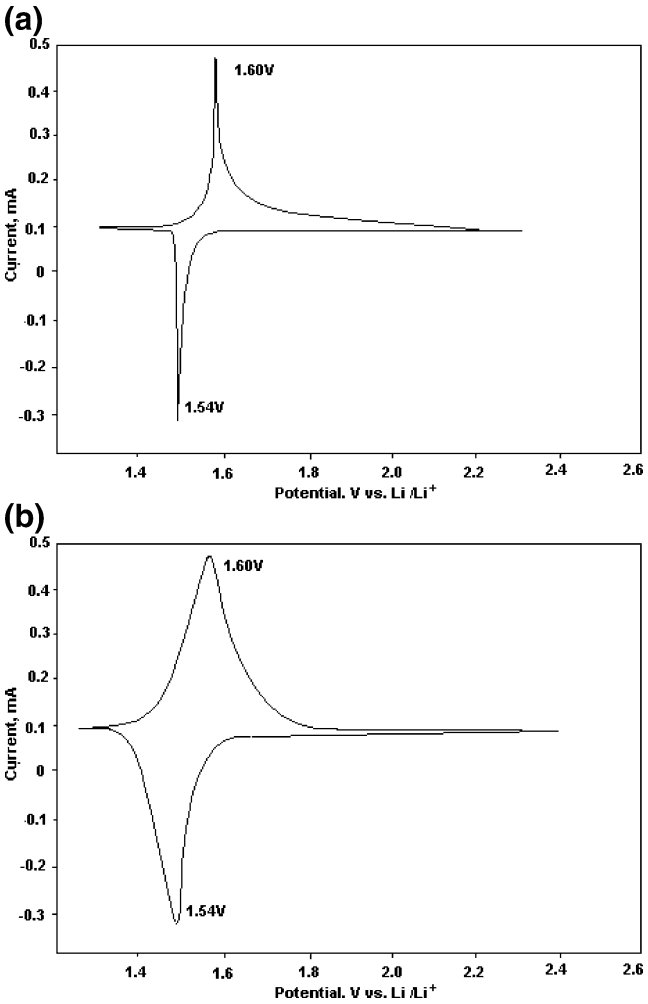

Fig. 5 (**a**) Cyclic voltammogram of $Li_4Ti_5O_{12}$ at the scan rate of 10 mV/s. (**b**) Cyclic voltammogram of $Li_4Ti_5O_{12}$ at the scan rate of 20 mV/s

0.0 to 3 V and then back to 0.0 V at a scan rate 10 and 20 mV/s, respectively. As per the following reaction

$$Li_4Ti_5O_{12} + 3e^- + 3Li^+ \rightarrow Li_7Ti_5O_{12}$$

Lithium insertion should occur at 1.54 V and extraction at 1.6 V for phase pure $Li_4Ti_5O_{12}$. CV studies had thus indicated that the synthesized compound is phase pure and free from anatase phase, which was established by the absence of peaks at 1.75 and 2.0 V vs Li/Li^+ [38].

This cyclic voltammogram was in good agreement with that of previous works, synthesized using different methods [12–19, 39].

4.2 Charge–discharge studies

These experiments were done from the point of view of some applications e.g. portable electronics where rapid charging may be just as important as high rate discharging. The discharge capacity of $Li_4Ti_5O_{12}/Li$ cell at various C

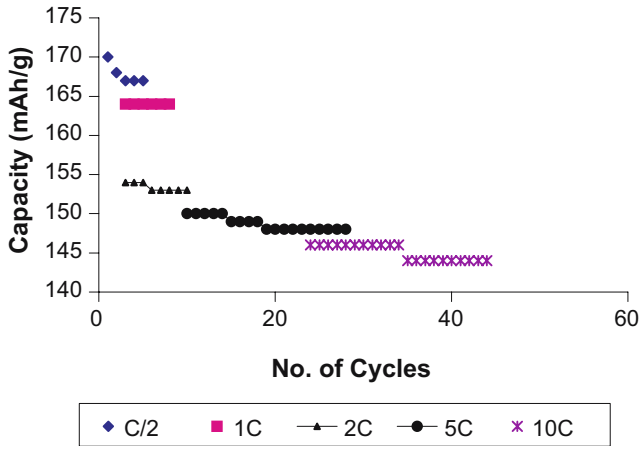

Fig. 6 Charge–discharge capacities of $Li_4Ti_5O_{12}$ at various C rates

rates is presented in Fig. 6. The charge discharge studies were carried out with 2016 coin cell. The electrode area was 1 cm^2 and the active material on the electrode was 20 mg. The discharge current was maintained at 3 mA for C rate discharge. The discharge current was maintained accordingly for other rates of discharge. The discharge capacities of the $Li_4Ti_5O_{12}$ electrode delivered a capacity of 154 $mAhg^{-1}$ at the 2 C rate, 164 $mAhg^{-1}$ at the C rate and 170 $mAhg^{-1}$ at C/2 rate. The initial open circuit voltage was 2.9 V for $Li_4Ti_5O_{12}$ fired at 800 °C. The discharge test was carried out between 2.5 and 1.0 V and the voltage was dropped quickly down to below 2 V and decreases further as the reaction proceeded until the voltage reaches about 1.51 V, after which the voltage was almost constant displaying the characteristic discharge plateau for $Li_4Ti_5O_{12}$. This initial rapid loss in capacity has already been observed for sol–gel derived $Li_4Ti_5O_{12}$ [40] and for the material prepared with the high-energy ball milling method [26].

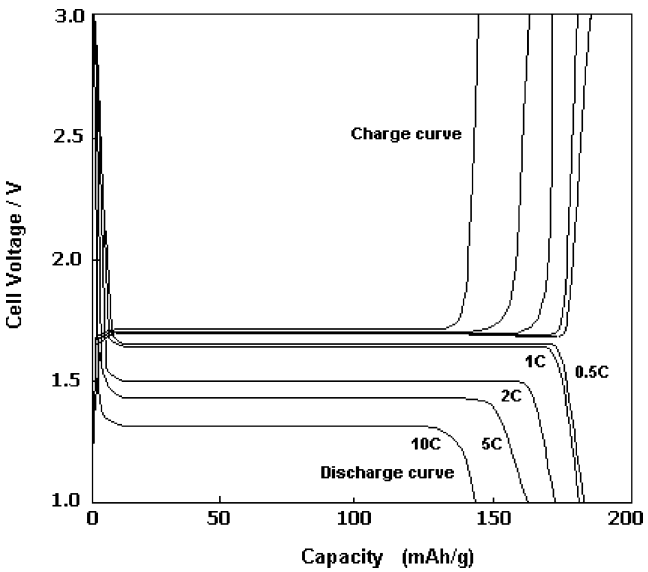

Fig. 7 Charge–discharge curves of $Li_4Ti_5O_{12}$ at 20 μ A/cm^2

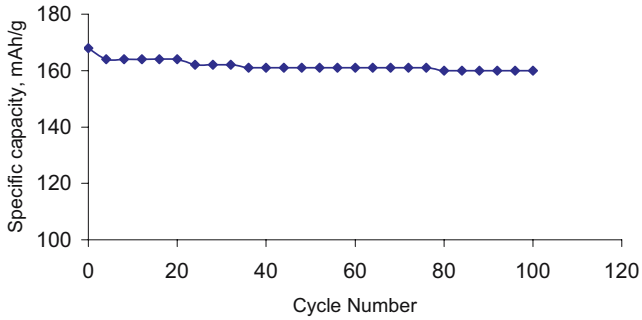

Fig. 8 Charge–discharge cycles of $Li_4Ti_5O_{12}$/Li cell at 1 C rate

Figure 7 shows the charge–discharge curves of $Li_4Ti_5O_{12}$ at 20 μ A/cm^2 in a mixed solvent of ethylene carbonate and diethyl carbonate containing 1.0 $moldm^{-3}$ $LiPF_6$. The discharge and charge curves were very flat and their working potentials were around 1.55 V. This potential range corresponds to the free energy change of $Li_4Ti_5O_{12}$ as reported earlier [10, 13–15, 41]. Figure 8 shows the capacity (mAh/g) up to 100 cycles for the discharge conducted at 1 C rate. It is clear from the figure, no significant difference can be detected in the charge–discharge up to 100^{th} cycle, exhibiting very stable cycle characteristics.

In general for a lithium ion cell, there is no possibility of Li plating during high rate discharge and as a result a symmetrical charge discharge behavior is expected and the Fig. 7 indicates the same and the charge discharge symmetry is not broken indicating even at high rate discharge the electrode polarization is in the opposite direction and the system is able to handle a far higher electrode polarization without any significant effect on utilization. The Figs. 7 and 8, indicates the effect of charge rate on the capacity for the cells. The rate of charge was increased as indicated on each figure in mA cm^{-2} and the discharge was performed at a low rate (Fig. 7) and the symmetry in the discharge and charge processes seems to have been preserved upto a rate of 10 C .At higher rates, capacity utilization on charge appears to be seriously lagging behind than for a corresponding discharge. Figure 9 shows the chrono potentiometric behavior of $Li_4Ti_5O_{12}$ at constant current density. The main process located at 1.55 V is evidenced and this corresponds to the insertion of one lithium per mole of oxides. The charge–discharge curves occur at these voltages show a reversible reaction. The fast charging is also reversible. The maximum reversible lithium insertion capacity determined from 2 C rate was 210 mC. Kalbac et al. [42] reported the maximum reversible lithium insertion capacity for the commercial $Li_4Ti_5O_{12}$, nanocrystalline $Li_4Ti_5O_{12}$ without hydrothermal and hydrothermally grown nanocrystalline as 260, 340 and 300 mC, respectively and they also reported 85 and 143 mC for the powders having surface area 4.6 and 135 m^2/g [43]. It is clear that our compound having better results when compared to commercial and nanocrystalline spinel.

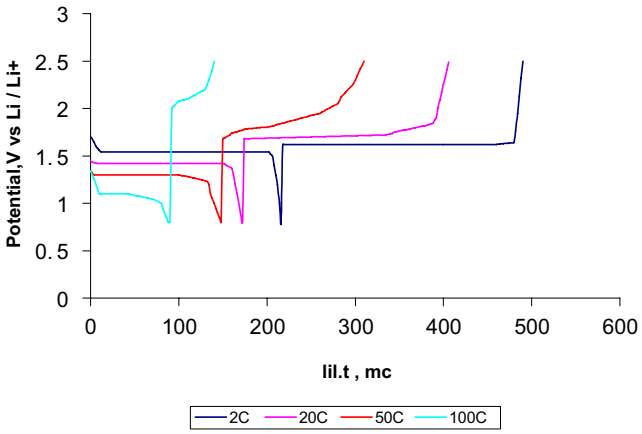

Fig. 9 Chrono potentiometric studies of $Li_4Ti_5O_{12}$

Pulsing capability of a battery becomes an important issue in application where battery power is delivered at high rate pulses for brief duration e.g. short cranking of an automobile and transmission of digital data in a personal communication system and hence pulse testing at different current densities such as 2, 5, 7, 5, 10, 20 mA cm^{-2} corresponding to 1 to 50 C rate was carried out and the material synthesized is able to provide up to 100 C rate which indicates the suitability for high rate capability. Galvanostatic chronopotentiometry curves adjusted to charge and discharge curves of 2, 20, 50, 100 C indicates that the particle size of synthesized material is tending towards nanorange in the thin film electrodes of 50–100 μm thick electrodes. As the charge transport increases at higher rates, these materials have infinite electrical resistivity in the starting nano lithiated state and the charge transport occurs via percolation among many necking nanoparticles of $Li_4Ti_5O_{12}$. The excellent charging rate of the synthesized cathode material demonstrates that the particle size is in the micrometer range.

From the chronoamperometic measurements the current after a potential step I, is controlled by diffusion and using the Cottrell equation.

$$I = S_{el}FD^{1/2}C\pi^{-1/2}t^{-1/2} \quad (3)$$

where S_{el} is the true (physical) electrode area, C is the concentration of Li^+ in the solid; D is the chemical diffusion coefficient. S_{el} can be chosen as BET area, C is the maximum concentration of mobile Li^+/Li in the $Li_4Ti_5O_{12}$ and this amounts to three extra Li^+ /Li ions in the $Li_4Ti_5O_{12}$ which amounts to be 21.9 mmole/cm^3. Experimental chronopotentiometric curves resemble that of nanocrystalline anatase [43–46]. Diffusion coefficients are calculated from the linear region for short time dependencies for the cathodic (insertion) process and this is in the range 10^{-13}–10^{-14} cm^2/s and this value is very much low compared to the normal diffusion coefficient value. Eventhough the surface area of the particle is 5.2 m^2/g, during charging/discharging at high rates, the particle size behaviour is approaching towards the values reported for nanocrystalline compound. This is understandable from the fact that Li^+–Li^+ repulsion for the same Li–Li insertion ratio will induce stress and consequently, the diffusion coefficients may drop by two to three order of magnitude if the particle size is decreased. If the current after a potential step I is controlled by diffusion the chrono potentiometric plot should formally obey the Cottrell equation.

The diffusion coefficient of ions through the electrolyte is not taken into account since ion diffusion in liquids (D_0 is of the order of 10^{-5} cm^2 S^{-1}) is generally much faster than in solid materials. It is reasonable to assume that lithium ions can readily cross the electrode/electrolyte interface and that diffusion through the solid electrode is rate limiting. For the cathodic reaction (Li^+ insertion) a diffusion coefficient 7.8×10^{-15} cm^2 s^{-1} was reported. [45] Our value 1.4×10^{-15} cm^2 s^{-1} thus is in agreement with the value as reported in [47]. Strictly speaking diffusion coefficients should only be determined for single phase systems, where the ion concentration and ion transport are governed by Fick's law. In a two phase system, ion transport is also determined by the velocity at which the phase front moves. This in turn depends on the activation energy of the phase transformation. Most of the equations used with standard techniques to measure ionic diffusivities are desired under the assumption of a Fickian diffusion process. Examples are the Cottrell's equation and also equation for Linear Sweep Voltammetry (LSV). These values calculated from these equations should be considered as apparent diffusion coefficients and in the present case also it may be conceived in this manner and whatever the values of diffusion coefficient reported may be considered as apparent diffusion coefficients.

4.3 Impedance studies

Generally these measurements have been used to study passivation film formation. In the absence of any surface layers the impedance of an insertion electrode can be interpreted in terms of a simple network consisting of the bulk electrolyte resistance, Rs, in series with a RC network. This network consists of two parallel current branches (1) a Faradaic current branch represented by a charge transfer resistance R_{ct} serially connected to diffusional impedance called Warburg impedance Zw and (2) a non Faradaic branch consisting of the double layer capacitance, Cdl. This network will yield one semicircle which will cut the real axis at R_b on the high frequency side and the other intersection point on the real axis at low frequency side R_b+R_{ct} values. Thus the impedance of the electrode can be interpreted in terms of a single circuit. A typical complex impedance diagram obtained in the frequency range 10^4–10^{-3} Hz for $Li_4Ti_5O_{12}$ is shown in Fig. 10. Figure 10

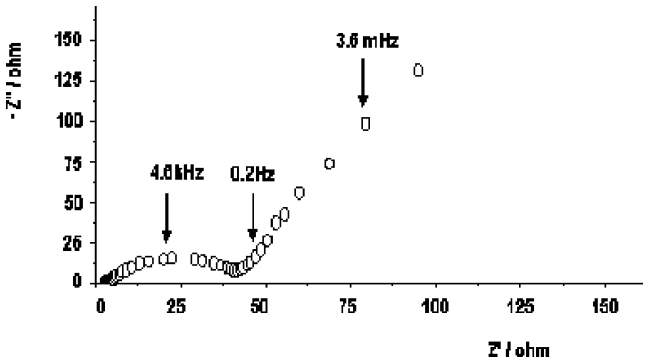

Fig. 10 Impedance diagram of $Li_4Ti_5O_{12}$

shows a semicircle and a straight-line obtained in the high and intermediate frequencies. The straight line corresponds to Warburg impedance due to a semi-infinite diffusion and the vertical line is due to a finite diffusion of Li^+ ion. The diameter of semicircle appearing at a higher frequency region corresponds to a charge transfer resistance. The chemical diffusion co-efficient was determined by Cabanel et al. [48] from the equation $D=\pi fl^2/1.94$, where f is transition frequency, l is the thickness of the material or film, D is the chemical diffusion co-efficient. The chemical diffusion co-efficient obtained from the above equation was 0.14×10^{-14} cm^2/s. It is well in agreement with the value obtained in the range 10^{-15}–10^{-14} cm^2/s [47]. As per the electrode area is concerned (BET Surface area 5.2 m^2/g) diffusion coefficient value should have been higher than the calculated values of 10^{-15} and this low value may be attributed to the deviation of the classical gradient like diffusion concept which cannot be transferred to lower particle size. This may also be true that Cottrell's formation may be phenomenologically valid at early stages of insertion in this material and the complex nature of insertion into porous electrode has to be studied in detail. Most probably the diffusion coefficient values reflect pseudo Cottrell behavior in a narrow time region which also depends on particle size. When particle gets smaller the interfacial region begins to dominate over the bulk.

Further $Li_4Ti_5O_{12}$ system displays only one semicircle and this further ascertained from the Bode plot (Z vs phase angle plot) where only one time constant is indicated and this suggests that there is no passivation which will be reflected from the second time constant of Bode plot. This suggests that $Li_4Ti_5O_{12}$ synthesized thus can be considered as a passivation free electrode [17]. This further suggests that this material will be useful to discharge at higher C rates compared with the material prepared conventionally.

4.4 Dielectric measurement

Dielectric constant values as a function of frequency at room temperature are shown in Fig. 11. The dielectric constant ε was calculated from the following equation $\varepsilon=Ct/\varepsilon_0A$, where C is the capacitance, ε_0 is the permittivity of empty space, t the film thickness, and A the area of the electrode. The dielectric constant was found to increase rapidly at low frequencies and more or less constant at higher frequencies which is depicted in Fig. 11. $Li_4Ti_5O_{12}$ shows low frequency dispersion of dielectric constant, which is attributed to the grain-to-grain contact. The dielectric constant is relatively stable up to a frequency of about 1,000 Hz, after which it increases abruptly at low frequency. The dielectric constant drops with increase in frequency whereas dissipation factor increases in the low frequency region. Both the curves meet at a frequency, which is called resonance frequency. This resonance frequency (1,500 Hz) may be due to electrode effects and internal interfacial barrier due to grain-to-grain contacts [49]. At high frequency (2.8–27.5 KHz), a loss tangent peak was found (the fig is not shown). This behaviour observed is probably associated with the sizes of the grains and to the interface between these grains. To understand the particle size effect, from the Cole Cole plot, the dielectric constant behaviour was studied and from these studies the following conclusions can be drawn. For samples in the present system the electrode contribution to the impedance data is ruled out on account of linear V-I characteristics of the samples. The total impedance has contributions of the grain and grain boundary. The resistance of these materials is very different but the dielectric constant is more or less equal ($\varepsilon_g\cong\varepsilon_{gb}$). Having understood this fact, the next step is to identify the resonance frequency where the power dissipation factor is minimum. For this, resonance frequency has to be found and this is defined as the meeting point of both the curves of variation of dielectric constant and dissipation factor with frequency. In the present case it was 1,500 Hz otherwise the response time , which is the inverse of resonance frequency, is 0.6 ms. This suggests that this electrode can be used as a high rate discharge electrode and also suggests that there is lesser inter-grain resistance which

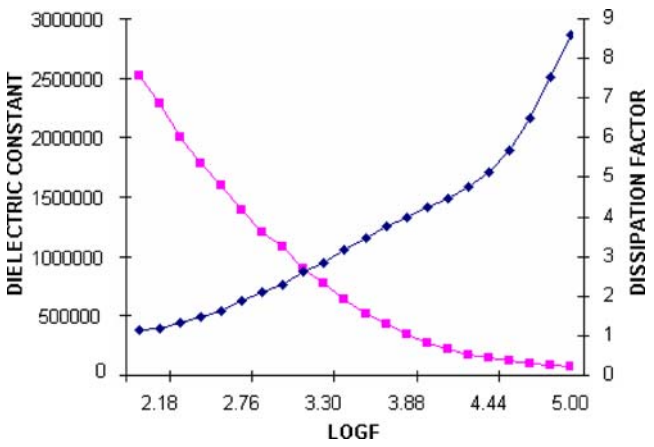

Fig. 11 Plot of log F vs dielectric constant and dissipation factor

will favor faster discharge compared to the powders prepared by conventional electrodes.

It is well known from many intercalation compounds that not all inserted ions can be extracted during the first cycle. A small percentage remains in the host lattice. This changes the properties of the material. From impedance analysis the measured capacitance at 50 KHz may be attributed to the space charge capacitance. In the present case the dielectric constant decreases with increase in frequency. This suggests that there is evidence for lithium intercalation by two modes as suggested for hydrogen intercalation in TiO_2. These are (1) irreversible filling with lithium, (2) reversible filling with lithium under potential control. Lithium is probably trapped as dangling bonds, in a similar way as in amorphous silicon, and thus the polarizability resulted is the cause of increase in dielectric constant at lower frequencies and this is what is depicted in the figure. As the frequency is increased sufficient number of ionized lithium ions can become degenerate and its conductivity will then increase since it becomes more metallic and dielectric constant decreases. Formation of Schottky barrier is very unlikely at the higher frequencies since there is no apparent reason for local charge build up at the interface and due to this the energy dissipation factor increases. There is a point where the energy dissipation factor will be optimum and this point is the resonance frequency where the curves the dielectric constant and dissipation factor meets.

5 Conclusion

Strain free $Li_4Ti_5O_{12}$ material was synthesized by a novel high temperature solid state quenching method. The material was used as an anode and tested for various electrochemical responses, which are assigned for rechargeable lithium batteries. XRD was used to assess the phase purity of the material. It was confirmed that phase pure $Li_4Ti_5O_{12}$ spinel was formed after 24 h of thermal treatment at 800 °C. Synthesized powder shows the maximum particle size distribution of about 1–2 μm. The $Li_4Ti_5O_{12}$ powder shows excellent reversible capacity at different depth of discharge and the material shows good cycle life without much capacity fade.

Acknowledgements We thank our Director, CECRI for his kind permission to publish this paper. We also thank DRDO for their financial support for this work.

References

1. T. Shodai, S. Okada, S. Tobishima, J. Yamaki, Solid State Ion. **86**, 785 (1996)
2. S. Suzuki, T. Shodai, Solid State Ion. **116**, 1 (1999)
3. J.J. Auborn, Y.L. Barbero, J. Electrochem. Soc. **134**, 638 (1987)
4. A. Watanabe, T. Kato, Jpn. Pat. Appl. **91–119**, 321 (1991) 23 April
5. E. Ferg, J. Guammow, A. de Kock, M.M. Thackeray, J. Electrochem. Soc. **141**, L147 (1994)
6. S. Huang, L. Kavan, I. Exnar, M. Gratzel, J. Electrochem. Soc. **142**, L142 (1995)
7. M.A. Cochez, J.C. Jumax, P. Lavela, J. Morales, J. Olivier-Foureade, J.L. Tirado, J. Power Sources **62**, 101 (1996)
8. S. Garmer, C. Bohnke, O. Bohnke, J.L. Fourquet, Solid State Ions. **83**, 323 (1996)
9. RK.B. Gover, J.R. Tolchard, H. Tukamoto, T. Murai, J.T.S. Irvine, J. Electrochem. Soc. **146**, 4348 (1999)
10. T. Ohzuku, A. Ueda, N. Yamamoto, J. Electrochem. Soc. **142**, 1431 (1995)
11. Y.H. Rho, K. Kanamura, M. Fujisaki, J. Hamagami, S. Suda, T. Umegaki, Solid State Ions. **151**, 151 (2002)
12. Y.H. Rho, K. Kanamura, T. Umegaki, Chem. Lett. 1322 (2001)
13. K. Kanamura, T. Umegaki, H. Naito, Z. Takehara, T. Yao, J. Appl. Electrochem. **31**, 73 (2001)
14. S. Ma, H. Noguchi, J. Electrochem. Soc. **148**, A589 (2001)
15. S. Bach, J.P. Pereira-Ramos, N. Baffier, J. Power Sources. **81–82**, 273 (1999)
16. D. Peramunage, K.M. Abraham, J. Electrochem. Soc. **145**, 2609 (1998)
17. S. Bach, J.P. Pereira-Ramos, N. Baffier, J. Mater. Chem. **8**, 251 (1998)
18. D. Peramunage, K.M. Abraham, J. Electrochem. Soc. **145**, 2609 (1998)
19. D. Peramunage, K.M. Abraham, J. Electrochem. Soc. **145**, 2615 (1998)
20. S. Takai, M. Kamata, S. Fujine, K. Yoneda, K. Kanda, T. Esaka, Solid State Ions. **123**, 165 (1999)
21. S. Schaanrer, W. Weppner, P. Schmid-Beurmann, J. Electrochem. Soc. **146**, 85 (1999)
22. K. Zaghib, M. Simoneau, M. Armand, M. Gauthier, J. Power Sources **81–82**, 300 (1999)
23. T. Ohzuku, K. Aryoshi, S. Yamamoto, Y. Makimura, Chem. Lett. 1271 (2001)
24. C.X. Wang, D.H. Bradhurst, S.X. Dou, H.K. Liu, J. Power Sources **83**, 156 (1999)
25. A. Deshanver, B. Raveau, Z. Sekkal, Mater. Res. Bull. **6**, 699 (1971)
26. K.M. Colbow, J.R. Dahn, R.R. Haering, J. Power Sources **26**, 397 (1989)
27. E. Ferg, R.J. Gummov, A. DeKock, M.M. Thackeray, J. Electrochem. Soc. **141**, L147 (1994)
28. M.R. Harrison, P.P. Edwards, J.B. Goodenough, Philos. Mag. **B52**, 679 (1985)
29. S.I. Pyun, S.W. Kim, H.C. Shin, J. Power Sources **81–82**, 248 (1999)
30. S. Scharner, W. Weppenr, P. Schmid Beurmann. J. Electrochem. Soc. **146**, 857 (1999)
31. K. Zaghib, M. Simoneu, M. Armand, M. Gauthier, Electrochim Acta, **50**, 263 (2004)
32. K. Zaghib, M. Simoneu, M. Armand, M. Gauthier, J. Electrochem. Soc. **145**, (1998)
33. S. Takai, M. Kamata, S. Fujine, K. Yoneda, K. Kanda, T. Esaka, Solid State Ions. **123**, 165 (1999)
34. G.G. Amatucci, F. Badway, A. Du Pasquier, T. Zheng, J. Electrochem. Soc. **148**, A930 (2001)
35. A. Du Pasquier, A. Laforgue, P. Simon, G.G. Amatucci, J.F. Fauvarque, J. Electrochem. Soc. **149**, A302 (2002)
36. S. Bach, J.P. Pereira-Ramos, N. Baffier, J. Power Sources **68**, 586 (1997)
37. S. Bach, J.P. Pereira-Ramos, N. Baffier, J. Mater. Chem. **8**, 251 (1998)

38. L. Kavan, M. Gratzel, Electrochem. Solid-state Lett. **5**, A39 (2002)
39. G.C. Allen, M. Paul, Appl. Spectrosc. **49**, 451 (1995)
40. M.G.S.R. Thomas, P.G. Bruce, J.B. Goodenough, J. Electrochem. Soc. **132**, 1521 (1985)
41. K. Kanamura, H. Naito, Z. Takehara, Chem. Lett. **45**, (1997)
42. M. Kalbac, M. Zukalova, L. Kavan, J. Solid State Electrochem. **8**, 1 (2003)
43. L. Kavan, J. Prochazka, T.M. Spitler, M. Kalbac, M. Zukalova, T. Drezen, M. Gratzel, J. Electrochem. Soc. **150**(7), A1000–A1007 (2003)
44. L. Kavan, J. Rathousky, M. Gratzel, V. Shklover, A. Zukai, J. Phys. Chem. B. **104**, 12012 (2003)
45. R. Vandekrol, A. Goosens, J. Schooman, J. Phys. Chem. B. **103**, 7151 (1999)
46. L. Kavan, K. Krtaochuvitova, M. Gratzel, J. Electrochem. Soc. **394**, 93 (1995)
47. P. Krtil, D. Fattachova, J. Electrochem. Soc. **148**, A1045 (2001)
48. R. Cabanel, G. Barral, J.P. Diard, B. Le Gorrec, C. Montella, J. Appl. Electrochem. **23**, 92 (1993)
49. P.C. Joshi, S.B. Krupanidhi, J. Appl. Phys. **72**, 5827 (1992)